J. Synchrotron Rad. (1998). **5**, 772–773

UV emission spectrometer using a non-periodic grating

H. Sato,[a,b]* T. Kotsugi,[a] S. Senba,[a] H. Namatame[b] and M. Taniguchi[a,b]

[a]*Faculty of Science, Hiroshima University, Kagamiyama 1-3, Higashi-Hiroshima 739-8526, Japan, and* [b]*Hiroshima Synchrotron Radiation Centre, Hiroshima University, Kagamiyama 1-3, Higashi-Hiroshima 739-8526, Japan. E-mail: sato@hisor.material.sci.hiroshima-u.ac.jp*

(*Received 4 August 1997; accepted 3 November 1997*)

A UV emission spectrometer using a non-periodic spherical grating has been designed, which can be attached to the linear or helical undulator beamlines of the HiSOR light source at the Hiroshima Synchrotron Radiation Centre. The useful range of emitted photons from 10 to 100 eV is covered by two gratings with nominal groove spacings of 1/600 and 1/1200 mm. The energy resolution with a 100 μm entrance slit width and the 1/600 mm grating is better than 0.2 eV below 50 eV.

Keywords: UV emission spectroscopy; non-periodic spherical gratings.

1. Introduction

Recently, soft X-ray emission spectroscopy using synchrotron radiation has been carried out by several groups (Callcott *et al.*, 1986; Nordgren *et al.*, 1989; Shin *et al.*, 1995). This spectroscopy provides new information on the electronic structure of materials through a second-order process, and inelastic scattering processes have been observed in the soft X-ray region in addition to the fluorescence process. Almost all of the groups carried out emission experiments in the soft X-ray region using a Rowland-type optical system; few studies have been performed in the UV region. In this study we have designed an experimental system for emission spectroscopy in the UV region (10–100 eV), which can be attached to the linear or helical undulator beamlines at the storage ring (HiSOR) of the Hiroshima Synchrotron Radiation Centre. The linear (helical) undulator emits linear (circular) polarized light in the energy region 25–70 eV (4–40 eV) for the first harmonics.

2. Optical system

The optical system of our UV emission spectrometer is schematically shown in Fig. 1. Throughout this paper we shall use the usual symbols and the coordinates shown in the figure. The optical system is composed of an entrance slit, a non-periodic spherical grating and a multichannel detector. r and α are fixed to be 350 mm and 85.3°, respectively. The two gratings with R = 5649 mm and a ruled area of 45 × 25 mm can be exchanged in vacuum. Their nominal groove spacings, d, are 1/600 and 1/1200 mm. The diffracted rays focus onto the multichannel plate in front of the one-dimensional position-sensitive detector. The area is 50 × 50 mm and the surface is CsI-coated in order to increase the quantum efficiency. The spatial resolution, Δl, is 125 μm. The detector moves along the straight line at y = −469 mm and covers a β region going from 85.3 to 67.3°. The available photon energy regions with 1/600 and 1/1200 mm gratings are 10–50 eV and 20–100 eV, respectively.

The optical system using the non-periodic spherical grating has been discussed by Harada & Kita (1980). We define the b_i parameters of the grating using the relation between the groove number, n, and the position, y, as follows,

$$n = \frac{1}{d}\left(y + \frac{b_2}{R}y^2 + \frac{b_3}{R^2}y^3 + \frac{b_4}{R^3}y^4 + \ldots\right). \quad (1)$$

If we expand the light path function as a power series of y and z, $F = r + r' + \sum F_{ij}y^i z^j$, $F_{10} = 0$ gives the grating equation. F_{20} is related to the focal condition, F_{02} to astigmatism, F_{30} to the coma-type aberration, and other F_{ij} terms to higher-order aberrations.

The focal point is derived from $F_{20} = 0$, *i.e.*

$$\frac{1}{2}\left(\frac{\cos^2\alpha}{r} - \frac{\cos\alpha}{R}\right) + \frac{1}{2}\left(\frac{\cos^2\beta}{r'} - \frac{\cos\beta}{R}\right) + \frac{b_2}{R}\frac{m\lambda}{d} = 0. \quad (2)$$

The focal curve for the non-periodic spherical grating becomes extremely different from the Rowland circle because b_2 is not zero. We choose b_2 so that the focal curve is almost straight because the surface of the photon detector is planar. Fig. 2 shows focal curves for selected values of b_2. The focal curve with b_2 = −9 is the straightest. The best value of b_2 is −8.9, taking Δl into account. On the other hand, we determined b_3 and b_4 to be 86.3 and −1349 so as to satisfy $F_{30} = F_{40} = 0$.

Here we emphasize that the optical system using a non-periodic spherical grating has two advantages compared with the Rowland-type optical system. Because the focal curve is almost

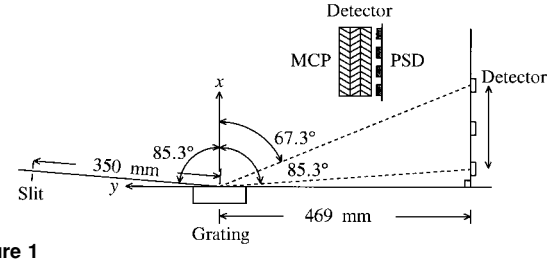

Figure 1
The designed optical system. The detector composed of the multichannel plate (MCP) and the one-dimensional position-sensitive detector (PSD) moves along and within the arrows.

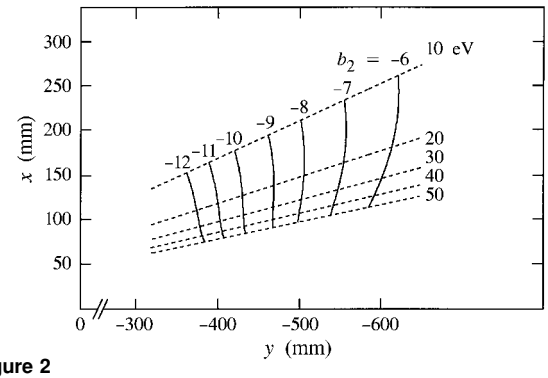

Figure 2
Focal curves for several values of b_2 (thick curve) with 1/600 mm grating. Dotted lines represent paths of the diffracted rays. The origin is at the centre of the grating.

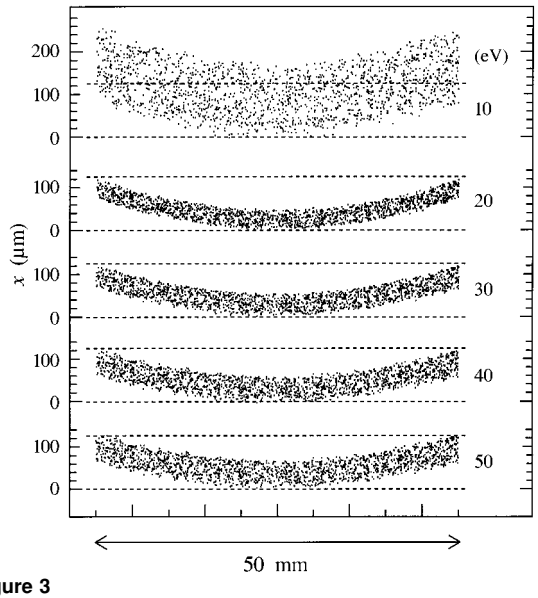

Figure 3
Photon images of the 100 μm entrance slit using the 1/600 mm grating. Dotted lines represent the spatial resolution of the detector.

straight and the detector moves along the straight line, it is easy to control the detector position and to scan the photon energy region. The other advantage is that the diffracted rays arrive almost normal onto the surface of the detector. This leads to an increased efficiency of photon detection compared with that of the grazing-incidence geometry of the Rowland mount.

3. Discussion

The image of photons on the surface of the detector has been investigated by ray tracing. Fig. 3 shows the images for several photon energies with the 100 μm slit and the 1/600 mm grating. The image for $E = 10$ eV is broader than for other energies because the focal point for $E = 10$ eV is about 7 mm in front of the detector moving line. The image has some aberration and is included within Δl, which is denoted by two dotted lines in the figure. Therefore, the resolution of the optical system is fixed by Δl. Fig. 4 shows the energy resolution determined by Δl. The resolution is better than 0.2 eV below $E = 50$ eV. As for energies below 13 eV, the resolution becomes somewhat worse than shown in Fig. 4 because the image becomes wider than Δl.

Fig. 5 schematically shows the experimental system of the UV emission spectrometer. It is composed of the analysis and preparation chambers. The UV emission spectrometer is attached to the analysis chamber, perpendicular to the synchrotron radiation port. An electron energy analyser is also mounted between the UV emission spectrometer and the synchrotron radiation port. Using the electron gun, X-ray tube and He discharge lamp we can perform resonant inverse-photoemission, resonant photoemission, UV and X-ray photoemission, as well as UV emission experiments. Furthermore, it is possible to carry out UV emission and photoemission coincidence experiments,

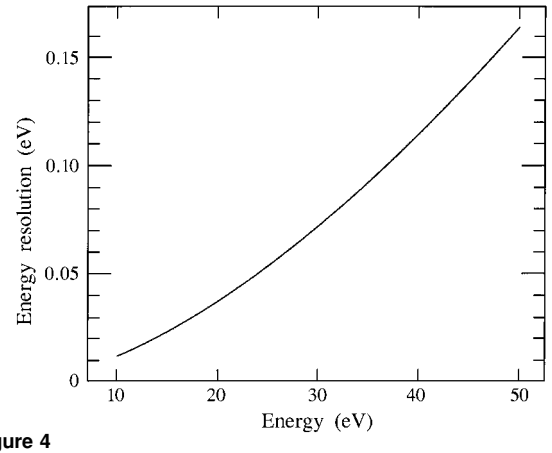

Figure 4
Energy resolution of the optical system with 1/600 mm grating derived from the spatial resolution of the detector.

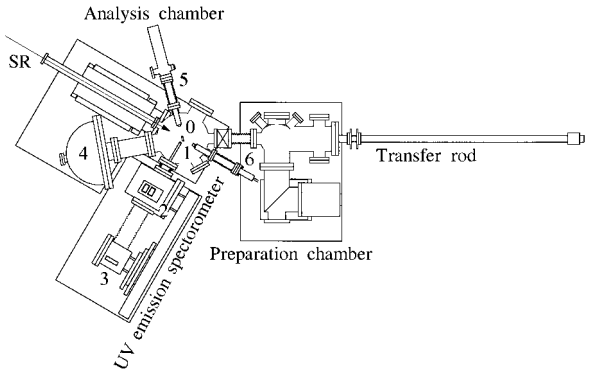

Figure 5
Outline of the experimental system for UV emission spectrometer. (0) sample; (1) entrance slit; (2) gratings; (3) detector; (4) electron energy analyser; (5) X-ray tube; (6) electron gun; SR = synchrotron radiation.

providing more detailed information on the electronic structure of the materials. A global study of the electronic structure of materials is planned.

The authors are grateful to Professor S. Shin, Professor T. Miyahara and Dr T. Kita for stimulating discussions of the optical system. They also thank J. Harada and K. Teramoto for design of the experimental system.

References

Callcott, T. A., Tsang, K. L., Zhang, C. H., Ederer, D. L. & Arakawa, E. T. (1986). *Rev. Sci. Instrum.* **57**, 2680–2690.
Harada, T. & Kita, T. (1980). *Appl. Opt.* **19**, 3987–3993.
Nordgren, J., Bray, G., Cramm. S., Nyholm, R., Rubensson, J.-E. & Wassdahl, N. (1989). *Rev. Sci. Instrum.* **60**, 1690–1696.
Shin, S., Agui, A., Fujisawa, M., Tezuka, Y. & Ishii, T. (1995). *Rev. Sci. Instrum.* **66**, 1584–1586.